Effects of Lateral Deformation by Thermoresponsive Polymer Brushes on the Measured Friction Forces

Shivaprakash N. Ramakrishna,*,[†] Marco Cirelli,[‡] Mohammad Divandari,[†] and Edmondo M. Benetti*,[†]

[†]Laboratory for Surface Science and Technology, Department of Materials, ETH Zurich, Vladimir-Prelog-Weg 5/10, 8093 Zurich, Switzerland

[‡]Department of Materials Science and Technology of Polymers, MESA + Institute for Nanotechnology, University of Twente, P.O. Box 217, 7500 AE Enschede, The Netherlands

⑤ *Supporting Information*

ABSTRACT: The nanotribological properties of hydrophilic polymer brushes are conveniently analyzed by lateral force microscopy (LFM). However, the measurement of friction for highly swollen and relatively thick polymer brushes can be strongly affected by the tendency of the compliant brush to be laterally deformed by the shearing probe. This phenomenon induces a "tilting" in the recorded friction loops, which is generated by the lateral bending and stretching of the grafts. In this study we highlight how the brush lateral deformation mainly affects the friction measurements of swollen PNIPAM brushes (below LCST) when relatively short scanning distances are applied. Under these conditions, the energy dissipation recorded by LFM is almost uniquely determined by stretching and bending of the compliant brush back and forth along the scanning direction, and it is not correlated to dynamic friction between two sliding surfaces. In contrast, when the scanning distance applied during LFM is relevantly longer than the brush lateral deformation, sliding of the probe on the brush interface becomes dominant, and a correct measurement of dynamic friction can be accomplished. By increasing the temperature above the LCST, the PNIPAM brushes undergo dehydration and assume a collapsed morphology, thereby hindering their lateral deformation by scanning probe. Hence, at 40 °C in water the recorded friction loops do not show any tilting and LFM accurately describes the dynamic friction between the probe and the polymer surface.
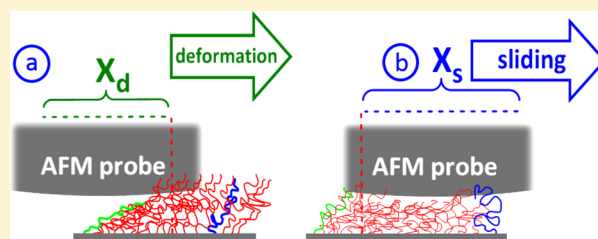
INTRODUCTION

The lubricating properties of hydrophilic polymer brushes have been increasingly attracting the attention of materials scientists[1−3] and tribologists[4−10] during the last two decades. Due to a combination of osmotic force and conformational entropy, densely grafted, swollen brushes can act as efficient boundary lubricants within aqueous media. This distinctive feature is revealed by a markedly low coefficient of friction (COF) recorded on brush-coated surfaces by micro- and nanotribometers,[11−16] surface forces apparatus (SFA),[17−19] and atomic force microscopy (AFM).[7,20−22] The frictional dissipation mechanisms as well as the effects of solvent quality on the nanotribological properties of polymer brushes were intensively studied both experimentally[23−28] and by simulation.[29−33] In particular, AFM-based techniques, such as lateral force microscopy (LFM), have been applied to study nanoscale friction generated between identical tribopairs, usually fabricated by grafting-to[34] of surface reactive copolymers.[25,35,36] Alternatively, LFM coupled to grafting-from methods, such as surface-initiated controlled radical polymerizations (SI-CRP), were employed to investigate the nanotribological properties of asymmetric tribopairs, concentrating on the interaction between sharp or colloidal AFM probes and relatively thick brush layers.[37−40]

A particular interest was devoted to the nanotribological properties of stimuli-responsive polymer brushes, and especially poly(*N*-isopropylacrylamide) (PNIPAM)-based grafts, which across the lower critical solution temperature (LCST) of 30−33 °C in water undergo a transition from swollen to dehydrated.[41,42] AFM methods were applied for measuring friction and nanomechanical properties with nanonewton resolution between a well-defined asperity and PNIPAM brushes presenting different thicknesses and grafting densities.[6,38,39,43−45] Although several studies helped dissecting the influence of these and other brush parameters on the nanotribological characteristics of PNIPAM brushes, a comprehensive and unambiguous understanding of the mechanics of interaction between the AFM probe and the brush surface across its LCST is still missing.

In this work, we demonstrate that the tendency of the PNIPAM grafts to be laterally deformed by the shearing AFM probe, which varies over the temperature-induced transition, determines brush-probe interactions, while a thorough understanding of brush lateral deformability enables the correct

Table 1. VASE and AFM Thickness Data for Thin and Thick PNIPAM Brushes in Dry Condition and in Milli-Q Water at 25° and 40°C

sample	ellipsometry			AFM		
	dry (nm)	water 25 °C (nm)	water 40 °C (nm)	dry (nm)	water 25 °C (nm)	water 40 °C (nm)
thin PNIAPM	11 ± 1	47 ± 6	13 ± 4	9 ± 3	33 ± 8	19 ± 10
thick PNIPAM	417 ± 4	1033 ± 22	486 ± 2	390 ± 6	655 ± 15	440 ± 12

measurement of friction by LFM. In particular, we address these issues by analyzing the frictional properties of PNIPAM brushes presenting different thicknesses below and above LCST.

We recently demonstrated that the measurement of friction between polymer brushes and an AFM probe includes different contributions originating from the reciprocal sliding of the two surfaces, plus the lateral bending and stretching of the tethered polymer chains.[38,46] The impact of this latter term on the measurement of friction can be conveniently visualized through the analysis of the friction "loops" recorded using LFM.[38,46] A tilted section of the loop is ascribed to the initial lateral deformation of the swollen brush, while a following, flat friction force trace is produced by the steady sliding of the probe on the polymer interface.

For PNIPAM brushes immersed in water below their LCST the lateral deformation by the compliant brush affects the dissipation recorded via the friction loops, and thus the applied scanning distance must be accordingly tuned to obtain a reliable value of COF.

In contrast, above LCST lateral deformability of the collapsed brush becomes irrelevant, and sliding of the probe on the brush interface uniquely determines the frictional dissipation.

■ EXPERIMENTAL SECTION

Synthesis of PNIPAM Brushes of Different Thicknesses. PNIPAM brushes of two different thicknesses were synthesized by surface-initiated atom radical polymerization (SI-ATRP) from initiator-functionalized silicon substrates (P/B < 100>, Si-mat, Germany) according to the previously reported procedure.[38] The catalyst system comprised CuBr (Sigma-Aldrich), CuBr$_2$ (Sigma-Aldrich) and N,N,N′,N″,N″-pentamethyldiethylenetriamine (PMDE-TA) (Sigma-Aldrich) in water/methanol mixtures.

The chemical composition of the so-fabricated PNIPAM brushes was confirmed by Fourier-transform infrared spectroscopy (FTIR) using a spectrometer (BIO-RAD FTS575C FTIR equipped with a nitrogen-cooled cryogenic cadmium mercury telluride detector) with spectral resolution of 8 cm^{-1}, applying 2048 scans for both the background spectra (performed on freshly cleaned silicon substrates) and the PNIPAM brush-modified samples. The surface-modification steps were also verified by contact angle (CA) measurements, using the sessile drop method. Both FTIR and CA characterizations are reported in the Supporting Information (Figure S1 and Figure S2).

Ellipsometry. The dry and wet thicknesses of PNIPAM brushes were measured by variable angle spectroscopic ellipsometry (VASE) using a Woolam ellipsometer (J.A. Woolam Co. U.S.) equipped with a custom-built, liquid cell and a temperature controller. Ψ and Δ as a function of wavelength (275−827 nm) were analyzed employing the package CompleteEASE (Woollam), using bulk dielectric functions for silicon, silicon dioxide, and water. The brush-underlying substrates were considered as silicon dioxide film on top of silicon substrate.

The analysis of the brush layers were performed using the Cauchy model: $n = A + B\lambda^{-2} + C\lambda^{-4}$, where A, B, and C represent the fitting parameters. We used $C = 0$ and assumed that the polymer films are fully transparent, i.e., the refractive index is a real quantity (the imaginary part is neglected). In the case of dry PNIPAM brushes, a homogeneous layer with a refractive index expressed with a single

Cauchy relation was considered. The films thickness d and the two Cauchy parameters A and B were used as fitting parameters. The dry thickness was obtained by performing the measurements at three different incident angles, namely 65°, 70°, and 75°.

For PNIPAM brushes immersed in water at 25 °C, we considered a density gradient across the film thickness employing a two-layer model to describe the optical response of the films (dense polymeric layer + graded polymeric layer) as it was previously described in detail.[38,39] For PNIPAM brushes immersed in water at 40 °C, a single-layer model was used.[47]

Atomic Force Microscopy Measurements. AFM measurements were carried out using a MFP-3D (Asylum Research, an Oxford Instruments company, Santa Barbara, CA, U.S.A.) equipped with a bio heater. Height micrographs of the brush surfaces were performed in milli-Q water below and above LCST of PNIPAM (25 and 40 °C) using AC mode. Cantilevers (SNL-10, D triangular) from Bruker Corporation, having a normal spring constant of ~0.06 N·m^{-1} were used for the tapping mode imaging in liquid.

Normal and lateral force measurements were carried out in milli-Q water at 25 and 40 °C, using a silica microsphere glued on a tip-less cantilever. The normal spring constant of the Au-coated, cantilever (NSC-12, Mikromash, Bulgaria) was measured by thermal-noise method[48] and the torsional spring constant was estimated according to the Sader's method.[49] Both the normal and the torsional spring constants of the cantilever were measured before attaching the colloidal microsphere. A silica sphere of radius ~8 μm (EKA chemicals AB, Kromasil R) was glued with a two component Araldite glue to the end of the tip-less cantilever by means of a home-built micro-manipulator.[50] The colloidal probe was treated with UV/ozone (BioForce Nanosciences) for 30 min just before the measurement.
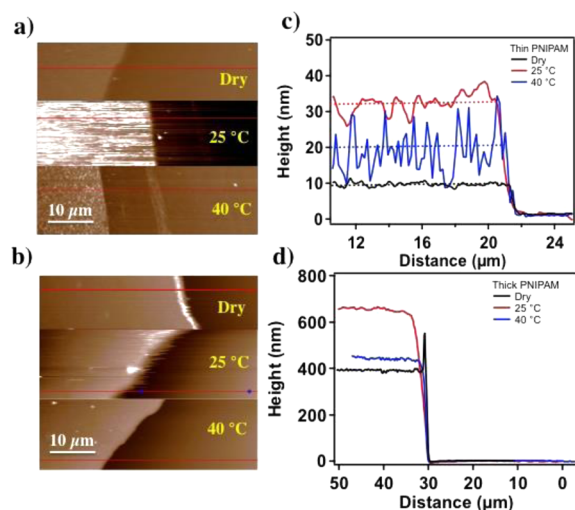
The adhesive properties of PNIPAM brushes, below and above LCST were examined by acquiring the force vs distance (F-D) curves (40 curves) over three different areas.

Lateral-force calibration was done by using the "test-probe method" described by Cannara et al.[51] A freshly cleaned, smooth edge of the silicon wafer was used as a "wall" for measuring the lateral sensitivity. A test probe (cantilever glued with a silica colloidal sphere of diameter around 40 μm) was moved laterally into contact with the wall. The lateral sensitivity of the photo detector was acquired by measuring the slope of the lateral deflection vs piezo displacement curve (a detailed procedure regarding the lateral force calibration is reported in the Supporting Information). Friction loops were recorded by lateral force microscopy (LFM) scanning the cantilever laterally over the brush surfaces. From the friction loops, the true friction values were obtained by averaging trace and retrace curves. Friction coefficient (COF) values were calculated by the slope of friction vs applied load plots assuming Amontons' law ($F = \mu L$), where F is friction force, μ is the coefficient of friction, and L is the applied load.

■ RESULTS AND DISCUSSION

PNIPAM brushes were synthesized from initiator-functionalized silicon substrates by SI-ATRP, varying the polymerization time and the catalyst/monomer mixture in order to obtain the desired brush thickness.[38] In particular, we aim to compare the frictional properties of relatively thin and thick PNIPAM brushes. Thus, two types of PNIPAM brushes alternatively presenting ellipsometric dry thicknesses of 11 ± 1 and 417 ± 4 nm (Table 1) were synthesized (named thin PNIPAM and thick PNIPAM, respectively). Fourier transform

infrared spectroscopy (FTIR) and water contact angle (CA) confirmed the successful formation of uniform PNIPAM films from initiator-functionalized silicon oxide substrates (data reported in the Supporting Information). The dry thickness values recorded by VASE were additionally confirmed by AFM step-height measurements, imaging the height difference between the brush surface and areas on the substrates where the films were mechanically removed by means of a plastic tweezer (Figure 1).[52] In addition, an average PNIPAM grafting

Figure 2. Tapping-mode AFM micrographs of PNIPAM brushes immersed in water. (a) and (b) thin PNIPAM brushes in water at 25 and 40 °C, respectively. (c) and (d) thick PNIPAM brushes in water at 25 and 40 °C, respectively. The same cantilever (SNL-10, D triangular) from Bruker Corporation was used for recording all the micrographs. This presented a normal spring constant of ∼0.06 N m^{-1}. The scanning speed was kept in all cases at 1 Hz. The amplitude set point and the drive amplitude were set at 0.7 and 0.3 V, respectively.
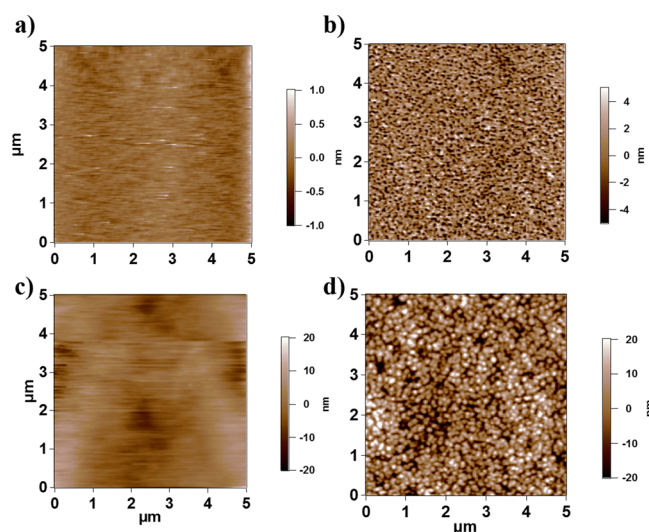

Figure 1. Tapping mode AFM micrographs (a,b) and corresponding section profiles (c,d) recorded over the "scratched" brush and the silicon surface for thin PNIPAM and thick PNIPAM. The red lines highlighted in the micrographs in a) and b) indicate where the section profiles reported in c) and d) were measured. The dotted lines in c) indicate the average values of thickness. The images were recorded under dry condition, and in Milli-Q water at 25° and 40 °C. A cantilever (SNL-10, D triangular) from Bruker Corporation, presenting a normal spring constant of ∼0.06 N m^{-1} was used for the tapping mode imaging in liquid. The scanning speed was kept at 1 Hz. The amplitude set point and the drive amplitude were set at 0.8 and 0.3 V, respectively.

density of 0.43 chains nm^{-2} was estimated by detaching the grafts via HF treatment, and subsequently analyzing the polymer sample by gel permeating chromatography (GPC; see the Supporting Information for details).

The morphology of thin and thick PNIPAM immersed in water both below (25 °C) and above the LCST (40 °C) were subsequently studied by tapping mode AFM (Figure 2). Below LCST, PNIPAM brushes showed smooth topographies, characteristic of swollen brushes, and presented a root-mean-square (RMS) roughness of 0.1 ± 0.02 and 1.5 ± 0.5 nm, for thin PNIPAM and thick PNIPAM, respectively (RMS values were calculated over an area of 5 × 5 μm^2).

Above the LCST, a marked increase of roughness was observed, due to the aggregation between PNIPAM grafts coupled to their vertical collapse. The formation of globular aggregates constituted by collapsed grafts was clearly observed for both thin and thick PNIPAM and produced an increase of RMS values that reached 2 ± 0.3 and 8 ± 1 nm, respectively (calculated over an area of 5 × 5 μm^2; Figure 2).[53]

The swelling properties of thin and thick PNIPAM in Milli-Q water were examined by VASE and AFM step-height measurements. The average thickness of PNIPAM brushes below LCST, was measured by VASE as 47 ± 6 and 1033 ± 22

nm, for thin and thick PNIPAM, respectively (Table 1). When compared to the corresponding dry thickness values, swelling ratios of 3.2 and 1.4 were calculated for the two polymer brush layers (calculated as the difference between swollen thickness and dry thickness, divided by dry thickness). Above the LCST, the temperature-driven collapse produced a marked decrease of the ellipsometric thicknesses, which at 40 °C in water reached 13 ± 4 and 486 ± 2 nm for thin and thick PNIPAM, respectively.

The thickness values obtained by VASE were subsequently confirmed by AFM step-height measurements. As shown in Figure 1 and Table 1, thin and thick PNIPAM brushes immersed in water at 25 °C showed height values of 33 ± 8 and 655 ± 15 nm, respectively. In contrast, at 40 °C the height of the brushes dropped to 19 ± 10 and 440 ± 12 nm, due to the collapse of the PNIPAM grafts. The deviation of these height values from the swelling data obtained by VASE was probably due to the compression of the brush by the AFM tip while scanning over the brush surfaces.[52] This effect resulted more marked at 25 °C in water, when the swollen and compliant brush can be compressed more easily by the AFM tip, originating an underestimate of the brush step-height.

Normal and Lateral AFM Force Measurements. The adhesive properties of thin and thick PNIPAM brushes, below and above LCST, were examined by acquiring force vs distance (F-D) curves by colloidal probe AFM (CP-AFM). As shown in Figure 3a, at 25 °C in water both thin and thick PNIPAM brushes showed repulsive interactions during the approach of the colloidal probe, due to the repulsion against compression exerted by swollen and densely grafted brushes.[53] Under these conditions, both thin and thick brushes displayed a slight hysteresis between the approaching and the retracting F-D profiles. This phenomenon was probably due to the stretching of the grafted chains up to several hundreds of nm from the
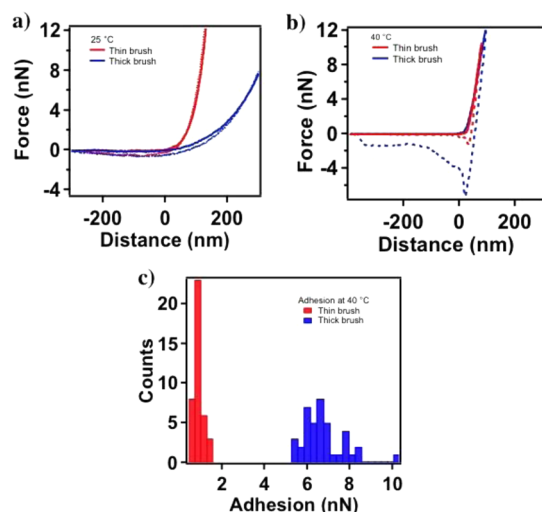
Figure 3. F-D curves for thin and thick PNIPAM brushes at 25 °C (a) and 40 °C (b). The solid lines indicate the approaching curves, while the dashed lines indicate the retracting profiles. In c) the distributions of adhesion forces recorded at 40 °C for thin (red) and thick PNIPAM (blue) brushes are reported. F-D curves were collected at a speed of 1 μm s^{-1} with a cantilever having normal spring constant of 1.57 N m^{-1} and presenting a silica colloid of 8 μm radius.

grafting surface during the retraction of the colloidal probe, as recently observed for similar PNIAPM brushes by Yu et al.[54]

Above the LCST, the dehydration of thin and thick PNIPAM brushes produced a marked steepening of the approaching F-D profiles (Figure 3b). In addition, the adhesive interactions recorded in the retracting F-D curve confirmed the presence of hydrophobic domains produced by the collapse of PNIAPM grafts above LCST.[53] Remarkably, an order magnitude increase in the adhesion force could be observed for thick PNIPAM grafts compared to thin ones. Namely, for thin PNIPAM brushes an average adhesion force of 0.8 nN was recorded, whereas thick PNIPAM brushes showed a much higher value of 6.3 nN, as shown in Figure 3c. The higher adhesion force recorded on thick-PNIPAM brushes was due to the increased contact area between the AFM colloid and the compressed brush. In addition, the long-range interactions recorded in the retraction profiles of the F-D curves were presumably generated by the vertical stretching of long polymer grafts within thick brushes by the retracting probe.

The nanotribological properties of the different PNIPAM brushes were subsequently investigated by LFM.

In Figure 4a, typical friction loops recorded on thin and thick PNIPAM brushes at 25 °C in water are reported. In the swollen state PNIPAM brushes present tilted friction loops. As previously described by us,[46,55] the tilted sections of the friction traces originate from the deformation (lateral bending and stretching) of swollen and compliant brushes by the scanning probe (X_d in Figure 4b,c). When the shear stress exerted by the probe overcomes the spring force of the deformed brush sliding finally occurs (X_s in Figure 4b,c), until scanning direction reversal and the consequent deformation and sliding toward the opposite direction.

Comparing the friction loops recorded for thin and thick PNIPAM brushes, a much lower contribution of tilting was observed for the thinner brushes with respect to the thicker ones. Namely, the lateral piezo extension corresponding to the tilted portion of the friction trace, X_d (or maximum lateral
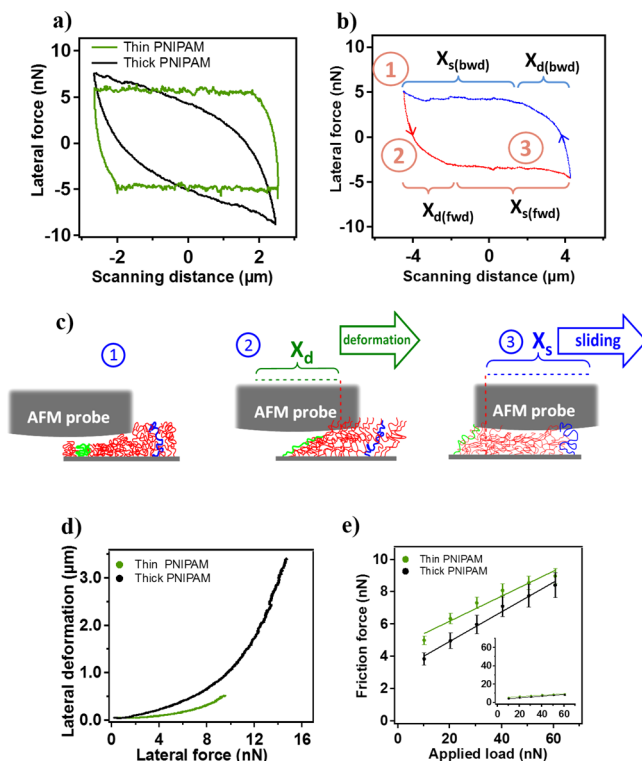
Figure 4. (a) Friction loops recorded by LFM on thin and thick PNIPAM brushes immersed in water at 25 °C for the applied load of 10 nN. In (b) a typical friction loop recorded on thick PNIPAM brushes is reported; the tilted portion (X_d) and the sliding portion (X_s) of the loop are also highlighted. A schematic representing brush deformation and sliding during scanning is reported in (c). In (d) the lateral deformation of thin and thick PNIPAM brushes is plotted against the recorded lateral force. (e) F_f-L profiles for thin and thick PNIPAM brushes recorded in water at 25 °C, the solid lines indicate the fit to the linear regression. In the inset, F_f-L profiles are reported applying the same vertical scale of Figure 5b, where the frictional properties of the PNIPAM brushes above LCST are plotted. The scanning distance and the scanning rate applied during CP-AFM friction measurements were 9 and 1 μm s^{-1}, respectively. The radius of the colloid used was 9 μm. The normal and torsional spring constants of the cantilever used were 0.263 N m^{-1} and 5.52 × 10^{-9} N m, respectively.

deformation) for thin PNIPAM brushes was estimated as 415 ± 30 nm, whereas thick PNIPAM showed a much higher X_d of 3010 ± 55 nm, as shown in Figure 4d.

Friction-vs-load (F_f-L) measurements further elucidated the frictional properties of thin and thick PNIPAM brushes. As reported in Figure 4e, at 25 °C the recorded friction force increased nearly linearly with the applied load. However, just a slight difference in COF was observed among thin and thick PNIPAM brushes (0.08 and 0.09 for thin and thick PNIPAM brushes, respectively).[40]

It is noteworthy to mention that although no clear adhesion could be recorded between the colloid and the swollen PNIPAM brushes, the F_f-L profiles measured at 25 °C did not clearly follow Amontons' law,[40] i.e., the recorded friction force was not directly proportional to the applied load. We believe that the observed slight deviation was possibly due to the interaction between the AFM colloid and the PNIPAM grafts, which was recorded as a slight but visible hysteresis between the approaching and retracting F-D profiles (Figure 3a). This interaction and the consequent stretching of the

chains affected the measured lateral force and resulted in a small variation of the slope of the F_f-L profiles.
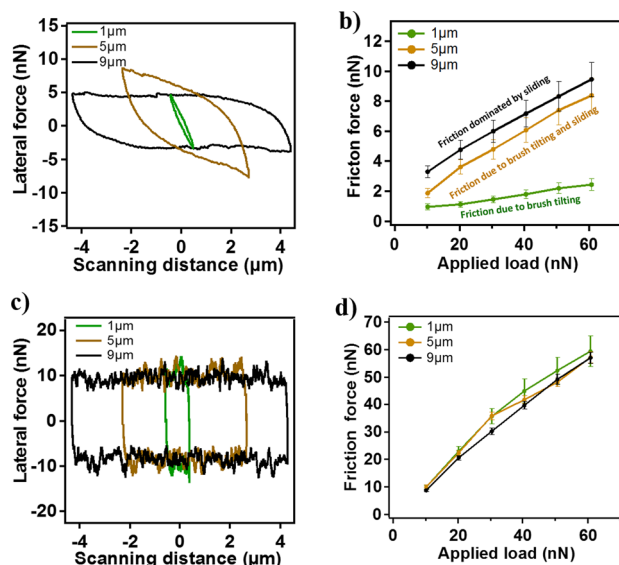
At 40 °C, the friction loops recorded on thin and thick PNIPAM brushes displayed very similar profiles, and no tilting effects were observed (Figure 5a). This result indicates that collapsed PNIPAM brushes could not be laterally deformed by the shearing probe, irrespective of their thickness.
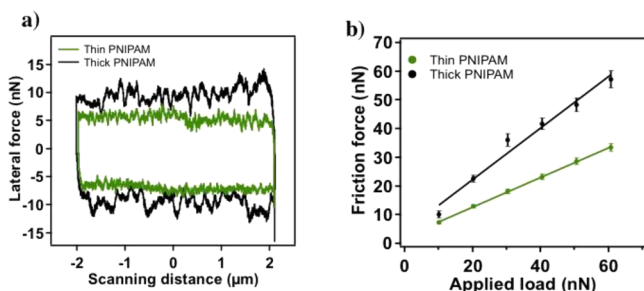
Figure 5. (a) Friction loops recorded on thin (green trace) and thick PNIPAM brushes (black trace) recorded at 40 °C in Milli-Q water by applying a normal load of 10 nN. (b) F_f-L profiles recorded on thin (green trace) and thick PNIPAM brushes (black trace) at 40 °C in Milli-Q water. The scanning distance and scanning rate applied during LFM were 9 and 1 μm·s^{-1}, respectively. The radius of the colloid used was 9 μm. The normal and torsional spring constants of the cantilever used were 0.263 N·m^{-1} and 5.52 × 10^{-9} N·m, respectively.

As expected, the F_f-L measurements for thin and thick PNIPAM brushes at 40 °C showed relevantly higher friction compared to 25 °C. However, as displayed in Figure 5b, thick PNIPAM brushes presented a steeper F_f-L profile if compared to the one recorded on thin PNIPAM analogues, with COF values of 0.9 and 0.5 for thick and thin PNIPAM brushes, respectively. The higher friction and COF observed for thick PNIPAM brushes in the collapsed state was likely due to the high adhesion force and increased surface roughness recorded above LCST for relatively thick PNIPAM brushes with respect to thinner ones.

Effect of Scanning Distance on Friction Measurements. In order to investigate the effect of brush lateral deformation on the friction measurements, we first analyzed the friction loops recorded on thick PNIPAM brushes at 25 °C, applying scanning distances of 1, 5, and 9 μm and maintaining a constant scanning speed of 1 μm s^{-1}. As displayed in Figure 6a, at the smallest scanning distance tested of 1 μm, the friction loop showed a completely tilted shape, as the lateral deformation of the swollen brush dominates brush–colloidal probe interaction, and sliding is never attained. Under these experimental conditions, the dissipation recorded via the friction loop (green trace in Figure 6a) is solely due to the back and forth bending and stretching of the swollen brushes. It is important to underling that at not slipping the apparent friction force induced by the cantilever torsion was due to the resistance by the PNIPAM grafts to bend and stretch along the lateral direction. An increase of the scanning distance to 5 μm causes the brushes to be initially deformed and stretched until static friction is overcome and sliding is finally gained (brown trace in Figure 6a). In this case, the dissipation measured via the friction loop originates from a combination of both brush stretching and sliding of the colloidal probe. A further increase of the scanning distance until 9 μm, which is a considerably larger distance than the maximum lateral stretching of the grafted chains, produces a friction loop presenting a tilted

Figure 6. (a) Friction loops recorded on thick PNIPAM brushes at 25 °C in water applying scanning distances of 1, 5, and 9 μm (individual curves are displayed separately in SI, Figure S6). (b) F_f-L profiles recorded on thick-PNIPAM brushes at 25 °C in water applying scanning distances of 1, 5, and 9 μm. Friction loops and F_f-L profiles recorded on thick PNIPAM brushes at 40 °C in water (c and d). The scanning velocity during the experiments was kept constant at 1 μm s^{-1}. The normal and torsional spring constants of the cantilever used were 0.263 N m^{-1} and 5.52 × 10^{-9} N m, respectively.

section after scanning direction reversal, followed by steady sliding of the colloid over several μm of piezo displacement. Thus, at relatively large scanning distances, the frictional dissipation is dominated by the sliding of the colloid over the brush surface (black trace in Figure 6a).

When a scanning distance of 5 μm is applied, a virtual increase in the recorded lateral force toward direction reversal is observed. We believe this phenomenon was due to the piling-up of the deformed grafts along the scanning direction, which caused an increase of the lateral force experienced by the AFM probe. Since the rate at which the deformed brushes are recovering their equilibrium conformation is presumably lower compared to the applied scan rate, this topographical change by the brush surface affected the friction measurements. As a confirmation of this assumption, we laterally scanned the same brush with a sharp tip and observed an increase of the recorded height values on the edges of the Z-sensor micrographs (Figure 7), indicating brush piling-up toward scanning direction reversal.

The comparison of the F_f-L plots recorded at the three different scanning distances studied highlights how a variation of brush-colloidal probe interactions can lead to different measurements of the COF. The lowest COF value of 0.03 was obtained in the case of 1 μm of scanning distance. Across this relatively short scanning distance, the measured friction force was solely due to the energy dissipation caused by the lateral bending and stretching of the swollen brush (Figure 6a green trace). A marked increase in friction, with average COF of 0.08 was observed for F_f-L profiles at 5 μm of scanning distance. In this particular case, the frictional energy dissipation recorded via the loops derived from the combination of brush lateral deformation and sliding (Figure 6a brown trace). In contrast, at the largest scanning distance of 9 μm the measured friction
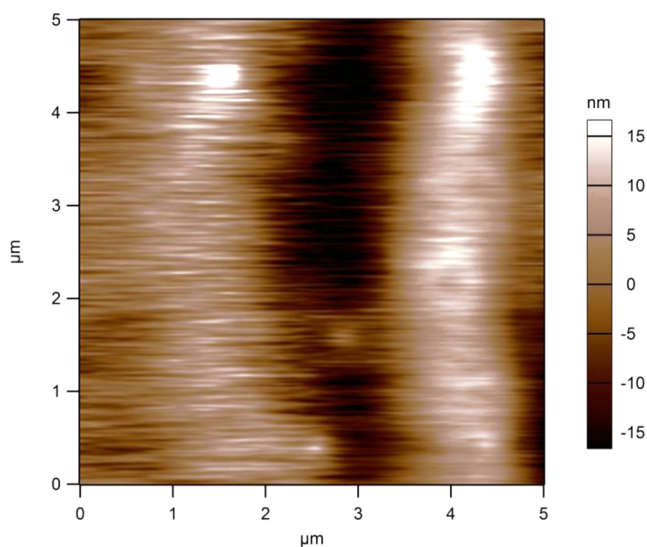
Figure 7. AFM height micrograph in contact mode for thick PNIPAM brushes immersed in Milli-Q water recorded at 25 °C with a sharp tip (SNL-10, applied load of ~20 nN).

Figure 8. (a) Friction loops recorded on thin PNIPAM brushes at 25 °C in water applying scanning distances of 0.5, 1.5, and 3 μm (individual curves are displayed separately in the Supporting Information). (b) F_f-L plots obtained for thick PNIPAM brushes at 25 °C in water applying 0.5, 1.5, and 3 μm of scanning distance. Friction loops and F_f-L profiles recorded on thin PNIAPM at 40 °C are displayed in (c) and (d). The scanning velocity during the experiments was kept constant at 1 μm s^{-1}. The normal and torsional spring constants of the cantilever used were 0.263 N m^{-1} and 5.52 × 10^{-9} N m, respectively.
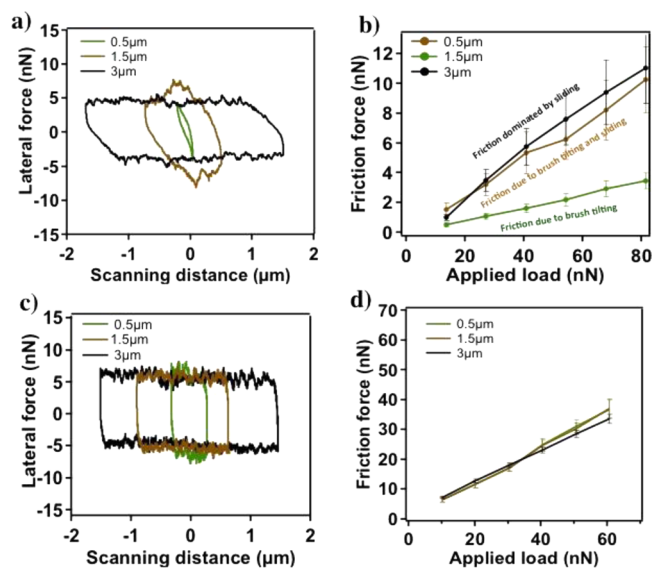
force is mainly determined by sliding of the colloid, and an average COF of 0.1 was measured (Figure 6b black trace).

The effect of brush lateral deformation on the measurement of friction becomes irrelevant at 40 °C, when PNIPAM brushes present a collapsed morphology. Under this condition, the friction loops do not show any tilt, and the F_f-L plots display a similar profile irrespective of the scanning distance applied. A constant COF of 0.9 is thus measured in all three cases, as indicated in Figure 6d.

Similar results are also obtained for thin PNIPAM brushes, although the occurrence of sliding was observed at a value of scanning distance relevantly shorter with respect to the more laterally deformable, thick PNIPAM brushes. As shown in Figure 8a, the transition from a completely tilted loop to a combination of tilting and sliding was recorded at 1.5 μm of scanning distance, while at larger distances sliding of the colloidal probe dominated the frictional properties of thin PNIPAM brushes. In this case, COF values of 0.04, 0.12, and 0.14 were obtained for 0.5, 1.5, and 3 μm of scanning distances, respectively (Figure 8b).

Similar to the result observed for thick PNIPAM brushes, at 40 °C the lateral deformation of thin brushes was completely suppressed and no tilting was observed in the recorded friction loops (Figure 8c). Hence, when recorded on the thin PNIPAM brushes above LCST, the F_f-L profiles measured across different scanning distances overlapped each other and indicated a constant COF of 0.5 (Figure 8d).

These results further confirmed that the contribution of brush lateral deformation to the energy dissipation can strongly alter the friction and thus COF values when the scanning distance applied during LFM is shorter or comparable to the maximum lateral deformation of the measured brush (X_d). This is particularly valid for highly swollen brushes, as in the case of PNIPAM immersed in water below its LCST, whereas in a bad solvent, the shearing probe can hardly laterally deform and stretch the collapsed and dehydrated brushes, and the frictional energy dissipation is mainly determined by the sliding of the probe over the brush surface.

CONCLUSION

In this report, we investigated the effect of the lateral deformation of a swollen brush by a shearing AFM probe on the measurement of friction forces. Brush lateral deformation, comprising bending and stretching of the grafts, can be quantified through the analysis of the friction force loops recorded by LFM. The tendency of a brush to be laterally deformed depends on brush parameters, such as the grafted-chain length (i.e., brush thickness) and it is particularly relevant and interesting in the case of thermoresponsive polymer brushes, being the swelling properties of such grafts precisely tunable by varying the temperature of the medium. For both thin and thick PNIPAM brushes immersed in water at 25 °C, the friction loops display a tilted behavior, with thicker brushes that can be laterally deformed more than thinner analogues. Thus, when relatively short scanning distances are applied for recording the friction loops, brush deformation mainly determines the frictional dissipation, while sliding of the colloid on the brush surface does not occur. Under these conditions, a relatively low COF was measured, which is uniquely originating from the bending and stretching back and forth of the swollen brushes. The application of scanning distances relevantly longer than the brush lateral deformation (expressed as X_d) produces friction loops displaying a tilted shape solely at scanning direction reversal, while sliding of the colloid on the brushes dominates the frictional dissipation recorded via the loops. In these cases, the slope of the F_f-L profiles as well as the derived COF values increase.

In contrast, due to brush dehydration and collapse above LCST, PNIPAM brushes cannot be laterally deformed at 40 °C in water. Tilting of the friction loops could not be observed under these particular conditions and the F_f-L profiles showed a

constant slope irrespective of the scanning distance applied for recording the loops.

Brush lateral deformation is thus proved to play a relevant effect on the measurement of friction and COF, especially when the measured brush is immersed in a good solvent and when relatively short scanning distances are applied during LFM. Our study demonstrates that while measuring COF, brush thickness, swelling properties and applied scanning distances are parameters to be carefully considered, as the simple recording of TMR (Trace minus Retrace) values from the friction loops may yield a conceptually wrong estimate of dynamic friction.

■ ASSOCIATED CONTENT

ⓢ Supporting Information

The Supporting Information is available free of charge on the ACS Publications website at DOI: 10.1021/acs.langmuir.7b00217.

> Additional experimental details and results as discussed in the text. (PDF)

■ AUTHOR INFORMATION

Corresponding Authors
*E-mail: shivaprakash.ramakrishna@mat.ethz.ch.
*E-mail: edmondo.benetti@mat.ethz.ch.

ORCID ⓘ
Edmondo M. Benetti: 0000-0002-5657-5714

Author Contributions
The manuscript was written through contributions of all authors. All authors have given approval to the final version of the manuscript.

Notes
The authors declare no competing financial interest.

■ ACKNOWLEDGMENTS

■ REFERENCES

(1) Jiang, S.; Cao, Z. Ultralow-Fouling, Functionalizable, and Hydrolyzable Zwitterionic Materials and Their Derivatives for Biological Applications. *Adv. Mater.* **2010**, *22* (9), 920−932.

(2) Navarro, M.; Benetti, E. M.; Zapotoczny, S.; Planell, J. A.; Vancso, G. J. Buried, Covalently Attached RGD Peptide Motifs in Poly-(Methacrylic Acid) Brush Layers: the Effect of Brush Structure on Cell Adhesion. *Langmuir* **2008**, *24* (19), 10996−11002.

(3) Krishnamoorthy, M.; Hakobyan, S.; Ramstedt, M.; Gautrot, J. E. Surface-Initiated Polymer Brushes in the Biomedical Field: Applications in Membrane Science, Biosensing, Cell Culture, Regenerative Medicine and Antibacterial Coatings. *Chem. Rev.* **2014**, *114* (21), 10976−11026.

(4) Li, A.; Ramakrishna, S. N.; Kooij, E. S.; Espinosa-Marzal, R. M.; Spencer, N. D. Poly(Acrylamide) Films at the Solvent-Induced Glass Transition: Adhesion, Tribology, and the Influence of Crosslinking. *Soft Matter* **2012**, *8* (35), 9092−9100.

(5) Lee, S.; Muller, M.; Ratoi-Salagean, M.; Voros, J.; Pasche, S.; De Paul, S. M.; Spikes, H. A.; Textor, M.; Spencer, N. D. Boundary Lubrication of Oxide Surfaces by Poly(L-Lysine)-G-Poly(Ethylene Glycol) (PLL-G-PEG) in Aqueous Media. *Tribol. Lett.* **2003**, *15* (3), 231−239.

(6) de Beer, S.; Kutnyanszky, E.; Schön, P. M.; Vancso, G. J.; Müser, M. H. Solvent-Induced Immiscibility of Polymer Brushes Eliminates Dissipation Channels. *Nat. Commun.* **2014**, *5*, 3781.

(7) Rosenberg, K. J.; Goren, T.; Crockett, R.; Spencer, N. D. Load-Induced Transitions in the Lubricity of Adsorbed Poly(L-Lysine)-G-Dextran as a Function of Polysaccharide Chain Density. *ACS Appl. Mater. Interfaces* **2011**, *3* (8), 3020−3025.

(8) Heeb, R.; Bielecki, R. M.; Lee, S.; Spencer, N. D. Room-Temperature, Aqueous-Phase Fabrication of Poly(Methacrylic Acid) Brushes by UV-LED-Induced, Controlled Radical Polymerization with High Selectivity for Surface-Bound Species. *Macromolecules* **2009**, *42* (22), 9124−9132.

(9) Chen, M.; Briscoe, W. H.; Armes, S. P.; Klein, J. Lubrication at Physiological Pressures by Polyzwitterionic Brushes. *Science* **2009**, *323* (5922), 1698−1701.

(10) Kobayashi, M.; Takahara, A. Tribological Properties of Hydrophilic Polymer Brushes Under Wet Conditions. *Chem. Rec.* **2010**, *10* (4), 208−216.

(11) Lee, S.; Spencer, N. D. Aqueous Lubrication of Polymers: Influence of Surface Modification. *Tribol. Int.* **2005**, *38* (11−12), 922−930.

(12) Nalam, P. C.; Clasohm, J. N.; Mashaghi, A.; Spencer, N. D. Macrotribological Studies of Poly(L-Lysine)-Graft-Poly(Ethylene Glycol) in Aqueous Glycerol Mixtures. *Tribol. Lett.* **2010**, *37* (3), 541−552.10.1007/s11249-009-9549-9

(13) Müller, M.; Lee, S.; Spikes, H. A.; Spencer, N. D. The Influence of Molecular Architecture on the Macroscopic Lubrication Properties of the Brush-Like Co-Polyelectrolyte Poly(L-Lysine)- G-Poly-(Ethylene Glycol) (PLL- G-PEG) Adsorbed on Oxide Surfaces. *Tribol. Lett.* **2003**, *15* (4), 395−405.10.1023/B:TRIL.0000003063.98583.bb

(14) Sakata, H.; Kobayashi, M.; Otsuka, H.; Takahara, A. Tribological Properties of Poly(Methyl Methacrylate) Brushes Prepared by Surface-Initiated Atom Transfer Radical Polymerization. *Polym. J.* **2005**, *37* (10), 767−775.

(15) Lee, S.; Muller, M.; Heeb, R.; Zürcher, S.; Tosatti, S.; Heinrich, M.; Amstad, F.; Pechmann, S.; Spencer, N. D. Self-Healing Behavior of a Polyelectrolyte-Based Lubricant Additive for Aqueous Lubrication of Oxide Materials. *Tribol. Lett.* **2006**, *24* (3), 217−223.

(16) Kobayashi, M.; Terayama, Y.; Hosaka, N.; Kaido, M.; Suzuki, A.; Yamada, N.; Torikai, N.; Ishihara, K.; Takahara, A. Friction Behavior of High-Density Poly(2-Methacryloyloxyethyl Phosphorylcholine) Brush in Aqueous Media. *Soft Matter* **2007**, *3* (6), 740−746.

(17) Drobek, T.; Spencer, N. D. Nanotribology of Surface-Grafted PEG Layers in an Aqueous Environment†. *Langmuir* **2008**, *24*, 1484.

(18) Raviv, U.; Giasson, S.; Kampf, N.; Gohy, J.-F.; Jérôme, R.; Klein, J. Lubrication by Charged Polymers. *Nature* **2003**, *425* (6954), 163−165.

(19) Tairy, O.; Kampf, N.; Driver, M. J.; Armes, S. P.; Klein, J. Dense, Highly Hydrated Polymer Brushes via Modified Atom-Transfer-Radical-Polymerization: Structure, Surface Interactions, and Frictional Dissipation. *Macromolecules* **2015**, *48* (1), 140−151.

(20) Müller, M. T.; Yan, X.; Lee, S.; Perry, S. S.; Spencer, N. D. Lubrication Properties of a Brushlike Copolymer as a Function of the Amount of Solvent Absorbed Within the Brush. *Macromolecules* **2005**, *38* (13), 5706−5713.

(21) Nalam, P. C.; Ramakrishna, S. N.; Espinosa-Marzal, R. M.; Spencer, N. D. Exploring Lubrication Regimes at the Nanoscale: Nanotribological Characterization of Silica and Polymer Brushes in Viscous Solvents. *Langmuir* **2013**, *29* (32), 10149−10158.

(22) Hurley, C. R.; Leggett, G. J. Influence of the Solvent Environment on the Contact Mechanics of Tip−Sample Interactions in Friction Force Microscopy of Poly(Ethylene Terephthalate) Films. *Langmuir* **2006**, *22* (9), 4179−4183.

(23) Klein, J.; Kamiyama, Y.; Yoshizawa, H.; Israelachvili, J. N.; Fredrickson, G. H.; Pincus, P.; Fetters, L. J. Lubrication Forces Between Surfaces Bearing Polymer Brushes. *Macromolecules* **1993**, *26* (21), 5552−5560.

(24) Tadmor, R.; Janik, J.; Klein, J.; Fetters, L. J. Sliding Friction with Polymer Brushes. *Phys. Rev. Lett.* **2003**, *91* (11), 115503.

(25) Brady, M. A.; Limpoco, F. T.; Perry, S. S. Solvent-Dependent Friction Force Response of Poly(Ethylenimine)-Graft-Poly(Ethylene Glycol) Brushes Investigated by Atomic Force Microscopy. *Langmuir* **2009**, *25* (13), 7443–7449.

(26) Raviv, U.; Tadmor, R.; Klein, J. Shear and Frictional Interactions Between Adsorbed Polymer Layers in a Good Solvent. *J. Phys. Chem. B* **2001**, *105*, 8125–8134.

(27) Klein, J.; Kumacheva, E.; Mahalu, D.; Perahia, D.; Fetters, L. J. Reduction of Frictional Forces Between Solid-Surfaces Bearing Polymer Brushes. *Nature* **1994**, *370* (6491), 634–636.

(28) Klein, J.; Perahia, D.; Warburg, S. Forces Between Polymer-Bearing Surfaces Undergoing Shear. *Nature* **1991**, *352* (6331), 143–145.

(29) Carrillo, J.-M. Y.; Russano, D.; Dobrynin, A. V. Friction Between Brush Layers of Charged and Neutral Bottle-Brush Macromolecules. Molecular Dynamics Simulations. *Langmuir* **2011**, *27*, 14599.

(30) Grest, G. S. Interfacial Sliding of Polymer Brushes: a Molecular Dynamics Simulation. *Phys. Rev. Lett.* **1996**, *76* (26), 4979–4982.

(31) de Beer, S.; Müser, M. H. Alternative Dissipation Mechanisms and the Effect of the Solvent in Friction Between Polymer Brushes on Rough Surfaces. *Soft Matter* **2013**, *9* (30), 7234–7241.

(32) Singh, M. K.; Ilg, P.; Espinosa-Marzal, R. M.; Kröger, M.; Spencer, N. D. Polymer Brushes Under Shear: Molecular Dynamics Simulations Compared to Experiments. *Langmuir* **2015**, *31*, 4798.

(33) de Beer, S.; Müser, M. H. Friction in (Im-) Miscible Polymer Brush Systems and the Role of Transverse Polymer Tilting. *Macromolecules* **2014**, *47* (21), 7666–7673.

(34) Zdyrko, B.; Luzinov, I. Polymer Brushes by the "Grafting to" Method. *Macromol. Rapid Commun.* **2011**, *32* (12), 859–869.

(35) Yan, X.; Perry, S. S; Spencer, N. D; Pasche, S.; De Paul, S. M; Textor, M.; Lim, M. S. Reduction of Friction at Oxide Interfaces Upon Polymer Adsorption From Aqueous Solutions. *Langmuir* **2004**, *20* (2), 423–428.

(36) Pettersson, T.; Naderi, A; Makuška, R.; Claesson, P. M Lubrication Properties of Bottle-Brush Polyelectrolytes: an AFM Study on the Effect of Side Chain and Charge Density. *Langmuir* **2008**, *24* (7), 3336–3347.

(37) Kitano, K.; Inoue, Y.; Matsuno, R.; Takai, M.; Ishihara, K. Nanoscale Evaluation of Lubricity on Well-Defined Polymer Brush Surfaces Using QCM-D and AFM. *Colloids Surf., B* **2009**, *74* (1), 350–357.

(38) Ramakrishna, S. N.; Cirelli, M.; Kooij, E. S.; Gunnewiek, M. K.; Benetti, E. M. Amplified Responsiveness of Multilayered Polymer Grafts: Synergy Between Brushes and Hydrogels. *Macromolecules* **2015**, *48* (19), 7106–7116.

(39) Chen, Q.; Kooij, E. S.; Sui, X.; Padberg, C. J.; Hempenius, M. A.; Schön, P. M.; Vancso, G. J. Collapse From the Top: Brushes of Poly-(N-Isopropylacrylamide) in Co-Nonsolvent Mixtures. *Soft Matter* **2014**, *10* (17), 3134–3142.

(40) Zhang, Z.; Morse, A. J.; Armes, S. P.; Lewis, A. L.; Geoghegan, M.; Leggett, G. J. Effect of Brush Thickness and Solvent Composition on the Friction Force Response of Poly(2-(Methacryloyloxy)-Ethylphosphorylcholine) Brushes. *Langmuir* **2011**, *27*, 2514.

(41) Smidsrød, O.; GUILLET, J. E. Study of Polymer-Solute Interactions by Gas Chromatography. *Macromolecules* **1969**, *2* (3), 272–277.

(42) Schmitt, F. J.; Park, C.; Simon, J.; Ringsdorf, H.; Israelachvili, J. Direct Surface Force and Contact Angle Measurements of an Adsorbed Polymer with a Lower Critical Solution Temperature. *Langmuir* **1998**, *14* (10), 2838–2845.

(43) de Beer, S. Switchable Friction Using Contacts of Stimulus-Responsive and Nonresponding Swollen Polymer Brushes. *Langmuir* **2014**, *30* (27), 8085–8090.

(44) Yu, Y.; Cirelli, M.; Kieviet, B. D.; Kooij, E. S.; Vancso, G. J.; de Beer, S. Tunable Friction by Employment of Co-Non-Solvency of PNIPAM Brushes. *Polymer* **2016**, *102*, 372–378.

(45) Sui, X.; Chen, Q.; Hempenius, M. A.; Vancso, G. J. Probing the Collapse Dynamics of Poly(N-Isopropylacrylamide) Brushes by AFM: Effects of Co-Nonsolvency and Grafting Densities. *Small* **2011**, *7* (10), 1440–1447.

(46) Li, A.; Ramakrishna, S. N.; Nalam, P. C.; Benetti, E. M.; Spencer, N. D. Stratified Polymer Grafts: Synthesis and Characterization of Layered 'Brush' and 'Gel' Structures. *Adv. Mater. Interfaces* **2014**, *1* (1), 1300007.

(47) Kooij, E. S.; Sui, X.; Hempenius, M. A.; Zandvliet, H. J. W.; Vancso, G. J. Probing the Thermal Collapse of Poly(N-Isopropylacrylamide) Grafts by Quantitative in Situ Ellipsometry. *J. Phys. Chem. B* **2012**, *116* (30), 9261–9268.

(48) Butt, H. J.; Jaschke, M. Calculation of Thermal Noise in Atomic-Force Microscopy. *Nanotechnology* **1995**, *6* (1), 1–7.

(49) Green, C. P.; Lioe, H.; Cleveland, J. P.; Proksch, R.; Mulvaney, P.; Sader, J. E. Normal and Torsional Spring Constants of Atomic Force Microscope Cantilevers. *Rev. Sci. Instrum.* **2004**, *75* (6), 1988–1996.

(50) Ducker, W. A.; Senden, T. J.; Pashley, R. M. Direct Measurement of Colloidal Forces Using an Atomic Force Microscope. *Nature* **1991**, *353* (6341), 239–241.

(51) Cannara, R. J.; Eglin, M.; Carpick, R. W. Lateral Force Calibration in Atomic Force Microscopy: a New Lateral Force Calibration Method and General Guidelines for Optimization. *Rev. Sci. Instrum.* **2006**, *77* (5), 053701.

(52) Benetti, E. M.; Reimhult, E.; de Bruin, J.; Zapotoczny, S.; Textor, M.; Vancso, G. J. Poly(Methacrylic Acid) Grafts Grown From Designer Surfaces: the Effect of Initiator Coverage on Polymerization Kinetics, Morphology, and Properties. *Macromolecules* **2009**, *42* (5), 1640–1647.

(53) Benetti, E. M.; Zapotoczny, S.; Vancso, G. J. Tunable Thermoresponsive Polymeric Platforms on Gold by "Photoiniferter"-Based Surface Grafting. *Adv. Mater.* **2007**, *19* (2), 268–271.

(54) Yu, Y.; Kieviet, B. D.; Liu, F.; Siretanu, I.; Kutnyanszky, E.; Vancso, G. J.; de Beer, S. Stretching of Collapsed Polymers Causes an Enhanced Dissipative Response of PNIPAM Brushes Near Their LCST. *Soft Matter* **2015**, *11* (43), 8508–8516.

(55) Gunnewiek, M. K.; Ramakrishna, S. N.; di Luca, A.; Vancso, G. J.; Moroni, L.; Benetti, E. M. Stem-Cell Clinging by a Thread: AFM Measure of Polymer-Brush Lateral Deformation. *Adv. Mater. Interfaces* **2016**, *3* (3), 1500456.